Vol. 08, No. 2 (2026) 1283-1298, doi: 10.24874/PES08.02B.017

Proceedings on Engineering Sciences

www.pesjournal.net

A COMPARATIVE FINITE ELEMENT INVESTIGATION OF VON MISES STRESS, DEFLECTION AND LOAD-CARRYING CAPACITY IN CHS AND CFST WARREN TRUSS STRUCTURES

Hanavadi Premakumar Sharath
Raviraj Shivaiah
Goud Mallesh[1]

Received 13.04.2026
Revised 21.05.2026
Accepted 02.06.2026

Keywords:

Warren truss, CHS, CFST, Finite element analysis, Deflection, Load carrying capacity, von Mises Stress

ABSTRACT

This study presents a comparative finite element investigation of von Mises stress, deflection and load-carrying capacity in Warren truss structures fabricated using Circular Hollow Sections (CHS) and Concrete-Filled Steel Tube (CFST) members. A total of twelve three-dimensional truss models conforming to Tata Structura specifications (IS 4923) were developed and analyzed using ANSYS Workbench under mid-point, two-point and uniformly distributed loading (UDL) conditions, evaluating the influence of the sectional area ratio ($2A_1/A_2$) and the depth-to-thickness ratio (h/t) on structural response. The steel was modelled with a Young's modulus of 210 GPa, yield strength of 310 MPa and Poisson's ratio of 0.3, while the concrete infill was assigned a compressive strength of 30 MPa and a Poisson's ratio of 0.25. Theoretical mid-span deflections for the CHS configurations ranged from 7.96 mm to 18.95 mm, with corresponding CFST values of 5.92 mm to 14.97 mm, reflecting stiffness improvements of 21.0% to 37.6%. Finite element results confirmed these trends, with CHS deflections of 9.20 mm to 21.01 mm and CFST deflections of 6.89 mm to 16.84 mm across all loading conditions, with deviations between theoretical and FEA results within 7.5–16.4%. Nonlinear analyses of the CFST configurations yielded ultimate load-carrying capacities of 355 kN, 245 kN and 600 kN under mid-point, two-point and UDL loading respectively, representing strength improvements of 49.0%, 37.7% and 26.4% over the equivalent CHS system. Average von Mises stresses across all configurations ranged between 242.86 and 307.14 MPa, remaining below the steel yield strength of 310 MPa and confirming structural safety within the elastic range. The results demonstrate that CFST Warren truss systems offer significant advantages in load-carrying capacity, stiffness and ductility, making them a viable and efficient alternative to conventional CHS trusses for bridge, industrial and infrastructure applications.

[1] Corresponding author: Goud Mallesh
Email: mallesh@sjce.ac.in

1. INTRODUCTION

Long span structural systems in bridges, roofs and towers demand a combination of lightness, load efficiency and constructional economy that conventional open sections struggle to achieve. Truss systems fabricated from hollow tubular sections address this challenge directly (Premakumar et al., 2026). Geometric efficiency and favorable strength to weight ratios allow slender members to carry heavy loads without the penalties associated with builtup sections. Among the available truss topologies, the Warren configuration is particularly effective because its alternating diagonal members form equilateral triangular panels in which every element resists pure axial force, eliminating bending and torsion from individual components and distributing loads uniformly across the system Satria et al. (2025). The Warren truss has consequently become the most widely adopted form in both pedestrian and vehicular bridge construction worldwide and its combination with tubular composite members represents a natural evolution toward higher structural performance.

Within the family of tubular members, Circular Hollow Sections (CHS) deliver uniform stress distribution, high torsional rigidity and inherent resistance to local buckling Rabi (2025), Timoshenko and Gere (2012). Concrete Filled Steel Tubes (CFST) extends these properties through composite action. The steel tube confines the infill concrete, elevating its compressive strength, while the concrete core restrains inward local buckling and contributes directly to axial and flexural stiffness. Furthermore, Han et al. (2014) provided a comprehensive review of CFST member behaviour under axial, bending, shear, and combined loading, establishing the composite mechanisms that continue to underpin current design practice. Beck et al. (2009) subsequently demonstrated, through Monte Carlo reliability analysis, that international code provisions for circular CFST columns exhibit inconsistent safety levels, thereby motivating a reliability based reassessment, a concern further reinforced by revised buckling design models for CHS beam columns, which offer improved safety margins over current provisions. Manikandann and Umarani (2021) confirmed that infill concrete type normal, high strength, lightweight or recycled aggregate measurably modifies confinement efficiency and ductility, while Pi et al. (2012) validated a simplified in plane strength model for CFST circular arches under combined bending and axial compression, demonstrating the versatility of CFST members across structural forms.

The application of CFST members to truss girder systems has been investigated through experimental and numerical programmes. Han et al. (2015) conducted the definitive bending tests on Warren type CFST chord to hollow brace trusses, establishing that concrete infill in the chords and the addition of a concrete slab deck each independently and significantly improve flexural stiffness and ultimate capacity. Simplified models verified against their data remain in common use. Huang et al. (2017) extended this work to pre stressed CFT truss girders, finding that both initial stiffness and ultimate strength increase with prestress level and shear span to depth ratio and that validated finite element models predict load deformation response reliably across configurations. Hu et al. (2023) conducted a parametric numerical study on steel tubular truss and concrete composite beams evaluating twelve variables slenderness, concrete grade, brace configuration and loading pattern and produced verified prediction methods for flexural stiffness and strength. On the composite slab side, AlObaidi et al. (2024) tested CFST beams composite with concrete deck slabs under four-point bending, demonstrating a 20% gain in flexural strength with higher strength concrete and a 40% gain when a channel section was introduced at the steel slab joint, with digital image correlation confirming that girder slab interaction governs the composite strain profile. Machacek and Cudejko (2011) examined longitudinal shear transfer and shear connector efficiency in composite steel concrete bridge trusses from elastic to ultimate states, concluding that joint behaviour dominates overall mechanical response a finding directly applicable to Warren CFST girder bridge design. Al Zand et al. (2020) complemented these studies by showing that internal steel stiffeners in cold formed square CFST beams delay local buckling and increase bending capacity by up to 45% and flexural stiffness by up to 60%, identifying stiffener configuration as a viable chord design parameter.

Connection performance and structural reliability are equally critical to truss level behaviour. Hou et al. (2013) quantified the influence of contact area, load eccentricity and concrete strength on the local bearing capacity of CFST chord to brace connections and proposed empirical design models. Abdelaal et al. (2024) presented finite element validated experiments on double bracket to CHS column joints under tensile loading, providing design recommendations for improved load transfer at CHS joint assemblies of the type found at Warren truss nodes. Singh et al. (2023) demonstrated that stiffened CFST columns with nanomaterial based infill achieve a 14% capacity gain through a propped stiffening scheme, confirming that section detailing exerts disproportionate influence on composite confinement. On reliability, Chen et al. (2019) developed a nonlinear Finite Element framework coupled with Monte Carlo simulation to assess CFST truss behaviour with random in situ geometric and material imperfections, proposing system resistance factors that establish a probabilistic design basis. The cyclic dimension of CFST response was addressed by Montuori et al. (2024), whose novel FE model validated against eight circular CFT tests accurately captures stiffness degradation, low cycle fatigue and failure mode progression under both monotonic and reversed cyclic bending, advancing the tools available for seismic assessment of CFST truss girders.

The design of CHS and CFST members and connections is governed by a suite of internationally recognised standards: AISC (2010, 2016) for hollow section connections and structural steel buildings Eurocode 3 and 4 (European Committee for Standardization, 2004, 2005a, 2005b) for composite, steel structures and joint design CIDECT (2008) for CHS joints under static loading and in the Indian context, IS 11384: 1985, IS 800: 2007 and IS 4923: 2017 for composite, general steel construction and hollow steel sections respectively. These standards provide a framework for member capacity, connection resistance and serviceability, but their integrated application to full Warren CFST truss systems where joint classification, composite efficiency and system level stability interact simultaneously has not been benchmarked against high fidelity experimental or numerical data. The absence of such validation leaves a critical gap between codal simplifications and the actual behaviour of this increasingly adopted structural form.

The literature revealed that full scale Warren CFST truss girder behaviour under combined loading remains uncharacterized composite efficiency of CFST over CHS chords is unquantified across truss geometries; reliability assessments specific to Warren CFST geometry with realistic imperfections are absent; and limited study has benchmarked finite element predictions against analytical theoretical values for this structural form.

The present study addresses these gaps through nonlinear numerical analysis in ANSYS Workbench, with explicit steel concrete interaction and geometric imperfection treatment, validated against Python generated theoretical calculations to establish reliable design tools for Warren CFST truss girders.

2. WARREN TRUSS GEOMETRY

A warren truss system consists of a repetitive series of equilateral or isosceles triangular units that are formed by inclined diagonal members connecting parallel top and bottom chords as shown in Figure. 1. This geometric configuration promotes efficient transfer of loads primarily through axial forces, thereby minimizing bending effects in individual members.

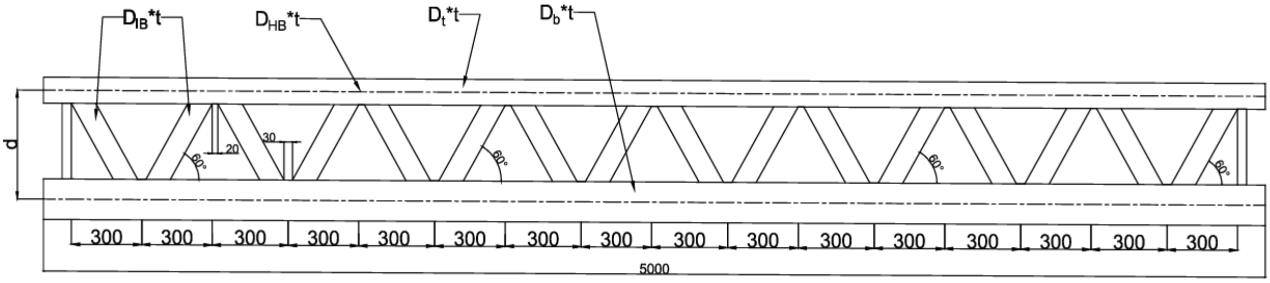

Longitudinal Section of Warren truss

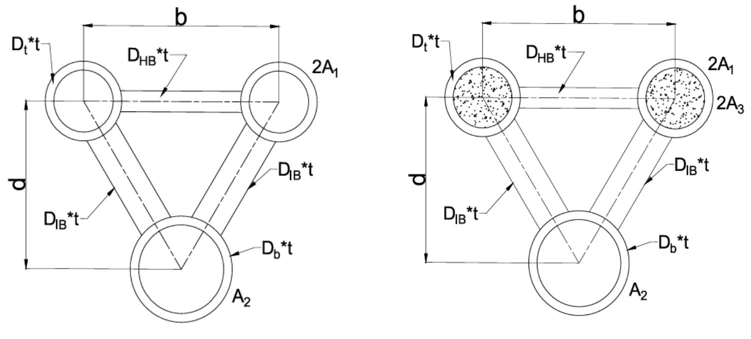

Circular Hollow Section (CHS) **Concrete filled Steel Tube (CFST)**

Figure 1. Warren truss configuration and cross sections

The design tables of Tata Structura Tata Steel - TSBU (2023) are widely used as they offer standardized properties for Hollow Steel Sections based on the Bureau of Indian standards codes. The use of these tables guarantees accuracy and reliability in the calculation of sections parameters, improving the efficiency of the design, optimization and safety of the structure.

A set of critical structural parameters, such as the moment of resistance, moment of inertia, Equal Area Axis, stress distribution, deflection and load carrying capacity, is evaluated under various loading conditions. The analytical treatment is organized into two separate cases based on the sectional area relationships: (i) $2A_1 < A_2$ and (ii) $2A_1 > A_2$ which correspond respectively to EAA positions on $h < t$ and $h > t$. This dual case approach is used to give a coherent basis for studying the influence of the sectional proportions on the strength and stiffness properties of the CHS truss system.

The CFST Warren truss structure is structurally similar; however, a fundamental difference lies in the construction of the top chord members, where the hollow sections are replaced with concrete filled steel tubes. This modification achieves composite action between the steel tube wall and the concrete core, because the confinement from the steel tube increases the compressive strength and stiffness of the infill and the concrete core increases the local buckling resistance and provides overall stability to the structure.

Implementing a parallel analytical approach, the CFST truss is evaluated using the same set of structural parameters under identical loading conditions. The two sectional area cases are re-examined by accounting for the increased cross sectional area and enhanced stiffness resulting from the concrete infill in the compression chord and the corresponding Equal Area Axis positions are determined accordingly. This systematic comparative assessment between CHS and CFST configurations clearly demonstrates how the incorporation of concrete into the top chord influences the load carrying capacity, stiffness distribution and overall structural response.

Table 1. Different warren truss configurations

Properties of CHS and CFST connections	Location of equal area axis	D_t*t	D_b*t	D_{IB}*t	D_{HB}*t	L_{eff}	d
$2A_1<A_2$	h<t	88.9*3.2	139.7*4.5	76.1*3.2	33.7*2.6	4800	400
		88.9*4	165.1*4.5				
	h>t	76.1*3.2	139.7*4.5				
		114.3*3.6	219.1*4.8				
		139.7*4.5	273*6				
$2A_1>A_2$	h<t	76.1*3.2	114.3*3.6				
		114.3*3.6	165.1*4.5				
		139.7*4.5	219.1*4.8				
	h>t	139.7*4.5	165.1*4.5				
		139.7*5.4	219.1*4.8				
		165.1*4.5	219.1*4.8				

3. ANALYTICAL ASSESSMENT OF EAA, MoR AND DEFLECTION IN CHS AND CFST SECTIONS

One of the most fundamental aspects of the structural evaluation of the Warren truss configurations is the analytical evaluation of the EAA, MoR and deflection. When calculating the properties of the sections, it is important to use the EAA as a reference, especially to find the location of the neutral axis and to calculate the bending resistance for symmetric and asymmetric cross sections. The moment of resistance indicates the resistance offered by the cross section to the imposed flexural demand while the deflection is a quantitative measure of the serviceability performance under the flexural demand imposed. It is therefore essential to be able to precisely determine these parameters to guarantee both structural safety and functional adequacy. The analytical behavior of these quantities is important in the context of CHS and CFST Warren truss systems; for these systems, the proportion and material composition of the sections vary considerably, and thus meaningful performance comparisons must be made based on reliable performance benchmarks.

3.1 Equal Area Axis for CHS and CFST

The EAA for different CHS and CFST configurations specified in Table 1 are determined using the following relations based on the criteria h < t and h > t and whether the axis passing through the top chord or bottom chord.

$$A = R^2 \cos^{-1}\left(\frac{R-h}{R}\right) - (R-h)\sqrt{2Rh-h^2} \quad (1)$$

$$A = \left\{R^2 \cos^{-1}\left(\frac{R-h}{R}\right) - (R-h)\sqrt{2Rh-h^2}\right\} - \left\{(R-t^2) * \cos^{-1}\left(\frac{R-h}{R-t}\right) - (R-t) * \sqrt{2(R-t)*(h-t)-(h-t)^2)}\right\} \quad (2)$$

3.2 Moment of Resistance for CHS and CFST

The moment of resistance defines a section's maximum capacity to withstand bending without failure. The centroidal distances y_1 through y_{12} from the Equal Area Axis (EAA) of all models are calculated using Equations 3 and 4, as illustrated in Figure 2. Further, the moment of resistance is calculated as per Equations 5 and 6.

$$\theta = 2\sin^{-1}\frac{\sqrt{2Rh-h^2}}{R} \qquad \breve{y} = \left(\frac{4R\,(\sin\frac{\theta}{2})3}{3(\theta-\sin\theta)}\right. \quad (3)$$

$$\theta = 2\pi - 2\sin^{-1}\frac{\sqrt{2Rh-h2}}{R};\ \breve{y} = \left(\frac{\frac{R2}{2}(\theta-\sin\theta)*4R\frac{(\sin\frac{\theta}{2})3}{3(\theta-\sin\theta)}}{\frac{R2}{2}(\theta-\sin\theta)-\pi(R-t)2}\right) \quad (4)$$

$$\mathrm{M_r}\ \text{for}\ (2A1 < A2) = \mathrm{C_1} * \mathrm{y_1} + \mathrm{C_2} * \mathrm{y_2} + \mathrm{T} * \mathrm{y_3} \quad (5)$$

$$\mathrm{M_r}\ \text{for}\ (2A1 > A2) = C * \mathrm{y_1} + \mathrm{T_1} * \mathrm{y_2} + \mathrm{T_2} * \mathrm{y_3} \quad (6)$$

Where;

$\mathrm{C_1} = \mathrm{F_{ysc}} * 2\mathrm{A_1}$; $\mathrm{C_2} = \mathrm{F_{ysc}} * \mathrm{A_{seg}}$

C = $F_{ysc} * (2A_1 - A_{seg})$

T = $\mathrm{F_{yst}} * (\mathrm{A_2} - \mathrm{A_{seg}})$

$T_1 = F_{yst} * A_{seg}$: $T_2 = F_{yst} * \mathrm{A_2}$

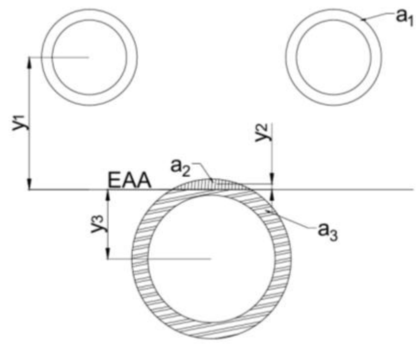

(a) $2A_1<A_2$ and h<t.

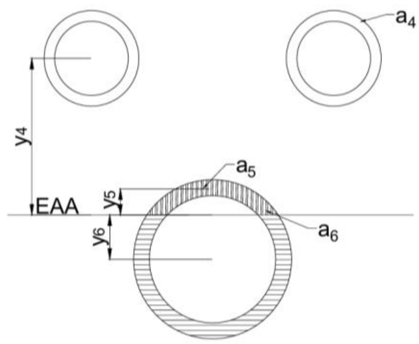

(b) $2A_1<A_2$ and h>t.

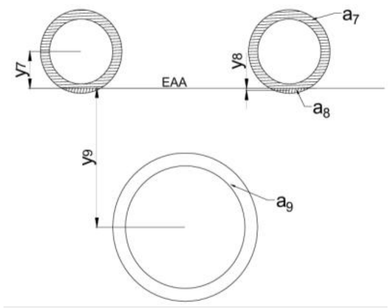

(c) $2A_1>A_2$ and h<t.

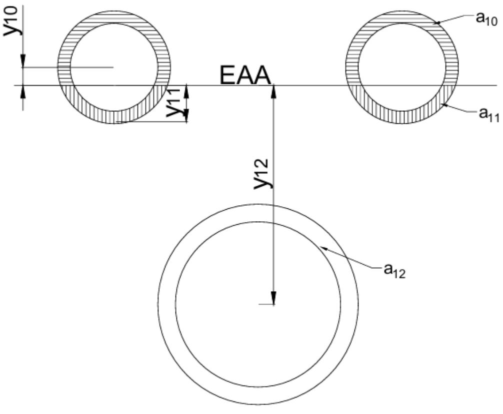

(d) $2A_1>A_2$ and h>t

Figure 2. Centroidal distance of chords from EAA for CHS Sections

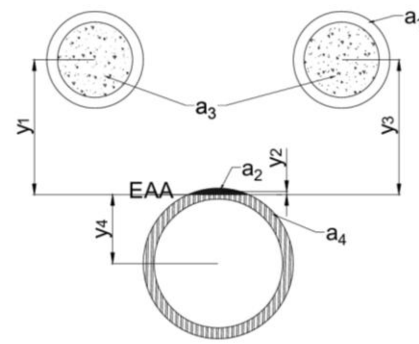

(a) $2A_1<A_2$ and h<t

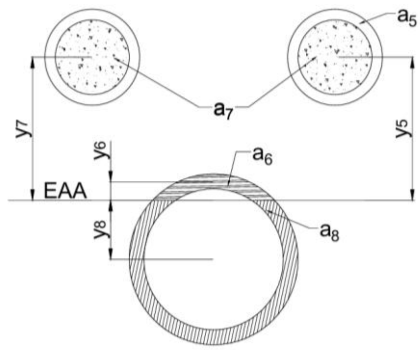

(b) $2A_1<A_2$ and h>t

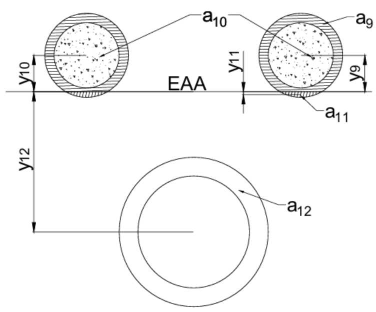

(c) $2A_1>A_2$ and h<t

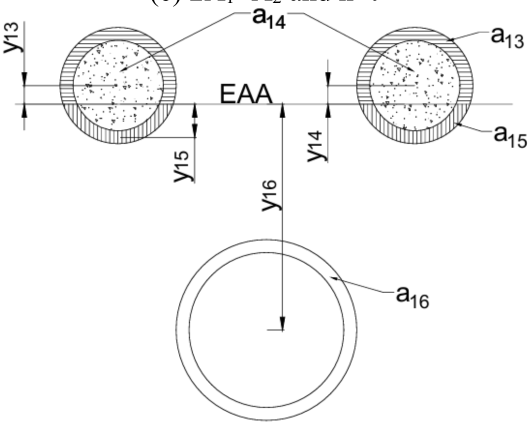

(d) $2A_1>A_2$ and h>t

Figure 3. Centroidal distance of chords from EAA for CFST Sections

Similarly, the centroidal distances from the EAA of all CFST models are calculated using Equations 3 and 4, as illustrated in Figure 3. Further, the moment of resistance is calculated per Equations 7, 8, 9, and 10.

$$M_r \text{ for } (2A_1 < A_2) = C_1 * y_1 + C_2 * y_2 + C_3 * y_3 + T * y_4 \quad (7)$$

$$M_r \text{ for } (2A_1 < A_2) = C_1 * y_5 + C_2 * y_6 + C_3 * y_7 + T * y_8 \quad (8)$$

$$M_r \text{ for } (2A_1 > A_2) = C_4 * y_9 + C_3 * y_{10} + T_1 * y_{11} + T_2 * y_{12} \quad (9)$$

$$M_r \text{for} (2A_1 > A_2 = C_5 * y_{13} + C_6 * y_{14} + T_1 * y_{15} + T_2 * y_{16} + T_3 * y_{17} \quad (10)$$

where;

$C_1 = F_{ysc} * 2A_1$; $C_2 = F_{ysc} * A_{seg}$

$C_3 = F_{ycc} * A_{concrete}$; $C_4 = F_{ysc} * (2A_1 - A_{seg})$

$C_5 = F_{yst} * (2A_1 - A_{seg})$; $C_6 = F_{ycc} * (A_3 - A_{seg})$

$T = F_{yst} * (A_2 - A_{seg})$; $T_1 = F_{yst} * 2A_{seg}$

$T_2 = F_{yst} * A_2$; $T_3 = F_{ycc} * 2A_{seg}$

3.3 Deflection for CHS and CFST

Deflection refers to the displacement of a structural member under loading. It is evaluated under uniformly distributed load (UDL), mid-point load and two-point loads to ensure serviceability compliance. The total truss weight for CHS and CFST models is determined by summing the contributions of their individual members, expressed as:

$$W_{DL} \text{for CHS} = (2\, L_t + L_b + L_i + L_h)\, \omega_1 \quad (11)$$

$$W_{DL} \text{for CFST} = (2\, L_t + L_b + L_i + L_h)\omega_1 + 2A_c\omega_2 \quad (12)$$

Equations 11 and 12 account for the combined self-weight of the top chord, bottom chord, inclined braces, horizontal braces and concrete in the top chords, each evaluated with respect to their respective lengths and the corresponding weight per unit length (ω), as specified for the respective cross-sections listed in Table 1. Further, the deflection of the truss is calculated based on the applied loads, including uniformly distributed loads (UDL), mid-point loads and two-point loads, in accordance with the required application and the self-weight of the members.

$$\delta = \frac{5*wl^4}{384*EI} \quad \text{for UDL} \quad (13)$$

$$\delta = \frac{wl^3}{48EI} \quad \text{for mid-point load} \quad (14)$$

$$\delta = \frac{wa*(3L^2-4a^2)}{24*EI} \quad \text{for two-point load} \quad (15)$$

3.4 Python Framework for EAA, MoR and Deflection

Given the large volume of data involved in the analysis, dedicated computational tools are developed using Python. The developed program improves computational efficiency, automates repetitive calculations and enables effective handling and processing of complex datasets. In addition, it enhances accuracy, reduces the possibility of manual errors and provides flexibility for implementing analytical procedures related to structural analysis. Owing to these advantages, the computational tool is employed in this research.

The equations presented in the previous sections are implemented through Python programming to determine the moment of resistance and deflection of the truss. The computed results are subsequently compared with the theoretical calculations to assess and validate the accuracy and reliability of the numerical approach.

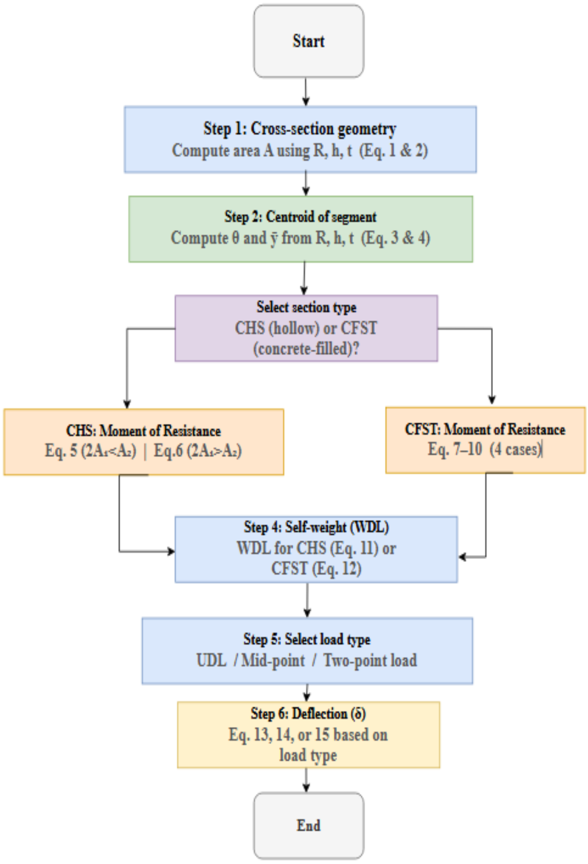

Figure 4. Flowchart for evaluating the moment of resistance and deflection for CHS and CFST sections

Figure 4 illustrates the step-by-step procedure for calculating the moment of resistance and deflection of CHS and CFST sections. The process begins with the cross-sectional geometry, where the area A is determined using radius R, depth h and wall thickness t, followed by the centroid calculation in which the subtended angle θ and centroidal distance ȳ are derived from the same geometric parameters. The moment of resistance for CHS is evaluated for two conditions, namely when $2A_1 < A_2$ and when $2A_1 > A_2$, while for CFST, the moment of resistance is determined through four cases accounting for the concrete infill contribution. The self-weight per unit length is then calculated for both CHS and CFST. The appropriate load type is subsequently selected and the deflection δ is computed accordingly, completing the structural design calculation.

4. 3-D MODEL OF WARREN TRUSS CONFIGURATIONS

Three dimensional (3D) solid models of the Warren truss configuration were developed using SOLIDWORKS parametric modeling software. The geometric parameters required for the modeling process were obtained from Table 2, which specifies the outer diameter and wall thickness of the top chord ($D_t \times t$), bottom chord ($D_b \times t$), diagonal braces ($D_{IB} \times t$) and horizontal braces ($D_{HB} \times t$), as well as the overall truss depth (d) and the center-to-center width between the top chords (b). Based on these specifications, a total of 12 distinct parametric models were generated to represent systematically varied design configurations. All models were constructed to reflect the exact member dimensions and nodal connectivity of the truss system and were subsequently saved in Parasolid (*.x_t) format and converted to IGES (*. iges) format for compatibility with finite element analysis software.

Figure 5(a) shows the CHS section, comprising the circular hollow steel tube without concrete infill, as adopted in the linear elastic analysis models. Figure 5(b) shows the CFST section, in which a solid concrete core is concentrically positioned within the circular hollow steel tube, clearly depicting the composite arrangement that governs the confinement behaviour and the nonlinear load-carrying response of the truss system.

Table 2. Cross-sectional dimensions for CHS and CFST truss configurations

Model Group	Model No.	Dt × t	$D_b \times t$	$D_{IB} \times t$	$D_{HB} \times t$	d	b
M1 ($2A_1 > A_2$, h < t)	M11	114.3 × 3.6	165.1 × 4.5	33.7 × 2.6	76.1 × 3.2	400	400
	M12						
	M13						
M2 ($2A_1 < A_2$, h > t)	M21	114.3 × 3.6	219.1 × 4.8	33.7 × 2.6	76.1 × 3.2	400	400
	M22						
	M23						
M3 ($2A_1 < A_2$, h < t)	M31	88.9 × 3.2	139.7 × 4.5	33.7 × 2.6	76.1 × 3.2	400	400
	M32						
	M33						
M4 ($2A_1 > A_2$, h > t)	M41	139.7 × 5.4	219.1 × 4.8	33.7 × 2.6	76.1 × 3.2	400	400
	M42						
	M43						

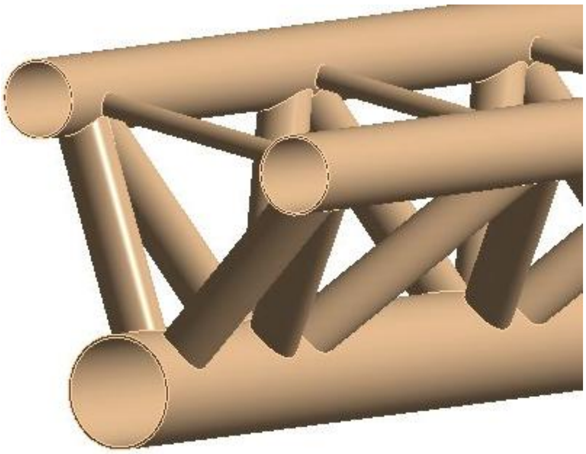

(a) CHS Section

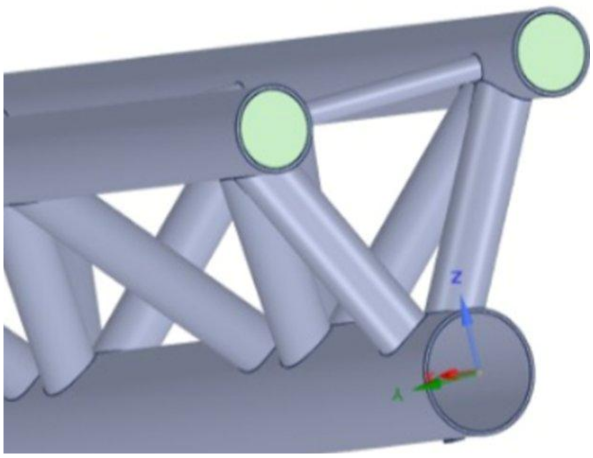

(b) CFST Section

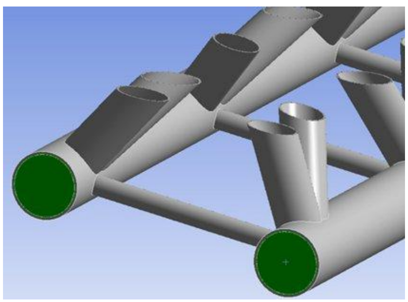

(c) Cut sectional view Braces

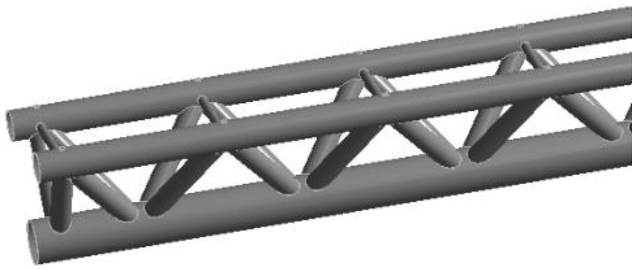

(d) 3 D model of Warren Truss

Figure 5. CHS, CFST, cut Sectional view of braces and 3-D model of Warren Truss

Figure 5 (c) represents the geometric relationship of the diagonal and horizontal bracing members to the chord members of the Warren truss. The figure is clearly intended to illustrate the inclination angle of the diagonal braces and spatial arrangement of the bracing system, both of which have a strong control over the load transfer mechanism and overall structural behaviour of the truss

Figure 5(d) shows the 3-D model of a representative Warren truss assembly that was created in SOLIDWORKS. The top chord, bottom chord, diagonal braces and horizontal braces, along with their nodal connectivity at the truss joints are shown. The global coordinate triad, as seen in the model, verifies the orientation of the axes which was used throughout the parametric modeling process. The 3-D model is used as the geometrically based models for linear elastic CHS and nonlinear finite elements analysis of CFST.

5. FINITE ELEMENT ANALYSIS OF WARREN TRUSS CONFIGURATIONS

The three-dimensional solid models of the Warren truss configurations, developed in SOLIDWORKS and saved in IGES (*. iges) format, were imported into ANSYS Workbench 2023 R1 via the Static Structural analysis system as shown in Figure 6. Upon import, the geometric integrity of each model was verified within the Design Modeler environment to ensure that all truss members, including the top chord, bottom chord, diagonal braces and horizontal braces, were correctly represented as individual solid bodies with proper nodal connectivity. For the CFST models, the steel tube and the concentric concrete core were defined as separate solid bodies and subsequently assigned a shared topology to enforce full displacement compatibility at the steel concrete interface, thereby simulating the composite interaction between the two materials.

Further, material properties were assigned to each solid body within the engineering data module of ANSYS Workbench. The circular hollow steel members were modelled as a linearly elastic isotropic material with a Young's modulus of 210 GPa, a Poisson's ratio of 0.3 and a density of 7850 kg/m³. For the CHS models subjected to linear elastic analysis, a bilinear isotropic hardening plasticity model was not applied and the response was evaluated within the elastic range. For the CFST models subjected to nonlinear analysis, the concrete infill was assigned a multilinear isotropic hardening material model based on the nonlinear constant confinement model, with a compressive strength of 30 MPa and a Poisson's ratio of 0.25. The steel tube in the CFST models was assigned a bilinear kinematic hardening model to capture the elastic plastic response under large deformations.

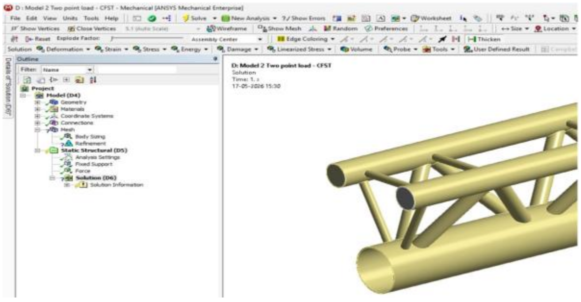

Figure 6. 3-D Model of Warren Truss in ANSYS Workbench Environment

The truss members were discretized using SOLID187 tetrahedral elements, selected for their suitability in accurately capturing stress concentrations and the curved geometric features inherent to the circular hollow section profiles. A mesh sensitivity study was conducted to determine the optimal element size and mesh refinement was subsequently applied at the nodal joint regions and at the steel–concrete interface, where stress gradients are most pronounced. A global element size of 10 mm was assigned to the chord members and 8 mm to the bracing members across all model configurations. The resulting mesh comprised approximately 180,000 elements for the CHS models and approximately 240,000 elements for the CFST models, with a minimum average element quality index of 0.82 maintained across all configurations, confirming mesh adequacy for reliable finite element analysis. The discretized finite element meshes of the representative CHS and CFST Warren truss models are presented in Figures 7(a) and 7(b), respectively, illustrating the mesh density distribution across the chord members, bracing members and nodal joint regions.

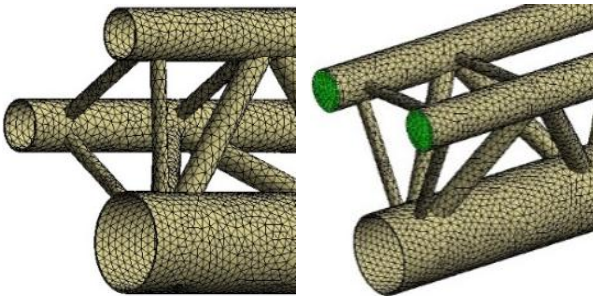

Figure 7 (a). CHS **Figure 7(b).** CFST

Figure 7. Meshed models of the CHS and CFST Warren truss

Boundary conditions were applied to replicate a simply supported configuration, with one end assigned a pinned support restraining translation in the X, Y and Z directions and the opposite end assigned a roller support restraining translation in the Y and Z directions while permitting longitudinal movement in the X direction, consistent with the idealized end conditions adopted for long-span truss systems. As described in Section 3.3, the calculated loads for UDL, mid-point load and two-point loads were applied to the top chord nodes of the truss as equivalent nodal forces. The applied load and displacement boundary conditions are presented in Figures 8(a) and 8(b), respectively. Load increments were applied in a stepwise manner for the nonlinear CFST analyses to facilitate convergence monitoring and to capture the progressive load–displacement response of the truss system.

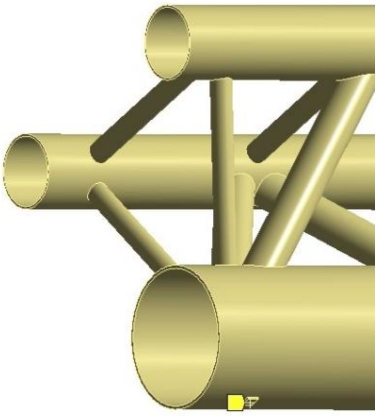

(a). Displacement boundary

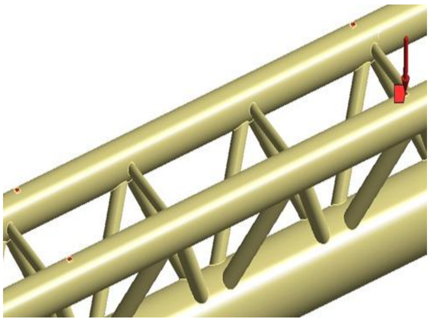

(b) Load boundary

Figure 8. Boundary conditions for truss configurations

For the CFST models, the steel–concrete interaction was modelled using a surface-to-surface contact pair, with the steel tube and concrete core designated as the contact and target surfaces, respectively. A bonded contact formulation was adopted for the linear range, while a frictional formulation with a coefficient of friction of 0.1 was applied for the nonlinear stage, with the augmented LaGrange algorithm enforcing the contact constraints. The nonlinear solution was executed using the Newton Raphson iterative method with large deflection effects activated, a load-stepping approach of 50 to 200 sub steps per increment and automatic time stepping enabled.

Upon solution convergence, the mid-span deflection and von Mises equivalent stress distribution were extracted for both the CHS and CFST model configurations using ANSYS Workbench. All post-processing results were tabulated and are presented in the results section for subsequent comparative analysis across the 12 model configurations and will be compared with the analytical solutions derived in Section 3.4.

6. RESULTS AND DISCUSSIONS

6.1 Theoretical and FEA Mid-Span Deflection for CHS and CFST Sections

This section presents the theoretical calculations for the Equal Area Axis (EAA), mid-span deflection and moment of resistance, incorporating the loading conditions defined in Section 3. Three model groups (M11, M12, and M13) are examined across twelve Warren truss configurations, each subjected to mid-point load, two-point load and uniformly distributed load (UDL) conditions.

For each configuration, the mid-span deflection and peak von Mises equivalent stress are reported and compared between the CHS and CFST configurations. The nonlinear load-deflection response of the CFST models at their respective ultimate load capacities is also examined.

Based on the EAA determined for each model, the moment of resistance is calculated for both the CHS and CFST chord members. The EAA consolidates the geometric and material properties of the cross-section into a single effective parameter, enabling the application of classical beam-truss theory to evaluate the flexural capacity of each configuration. The resulting theoretical mid-span deflections are subsequently validated against the corresponding FEA results, and the structural efficiency of the CFST system relative to the CHS system is evaluated across all loading scenarios.

Table 3 presents the theoretical mid-span deflections for the Warren truss models under different loading conditions, computed for both the CHS and CFST configurations. Under mid-point loading, model M11 recorded deflections of 17.96 mm and 11.20 mm for the CHS and CFST configurations respectively, reflecting a stiffness improvement of approximately 37.6% attributable to the enhanced axial stiffness of the composite section.

Table 3. Theoretical Mid-Span Deflections for CHS and CFST Warren Truss Configurations

Model	Load Type	Theoretical Deflection (mm)	Sections
M11	Mid-Point Load	17.96	CHS
M11		11.20	CFST
M12	Two Point Load	7.96	CHS
M12		5.92	CFST
M13	UDL	18.95	CHS
M13		14.97	CFST

For model M12 under two-point loading, deflections of 7.96 mm (CHS) and 5.92 mm (CFST) were obtained, corresponding to a reduction of 25.6%, with the lower absolute values consistent with the more favorable load distribution characteristic of this loading arrangement. Under UDL, model M13 exhibited the largest deflections among all cases, at 18.95 mm and 14.97 mm for the CHS and CFST configurations respectively, representing a reduction of 21.0%.

Across all loading scenarios, the CFST configurations consistently produced lower mid-span deflections than the corresponding CHS models, with reductions ranging from approximately 21% under UDL to 38% under mid-point loading. This confirms the beneficial effect of concrete infill in enhancing the flexural stiffness of the Warren truss system, with the greatest efficiency gain observed under concentrated loading conditions.

Figure 9 presents the FEA-predicted mid-span deflection contours for all Warren truss configurations across the three loading cases. Under mid-point loading (M11), the CHS and CFST configurations yield maximum deflections of 19.29 mm and 12.95 mm respectively, representing a reduction of approximately 32.9%. Under two-point loading (M12), the CHS and CFST configurations record deflections of 9.19 mm and 6.88 mm respectively, corresponding to a stiffness improvement of approximately 25.1% for the CFST system. Under UDL (M13), the CHS configuration records the largest mid span deflection among all loading cases at 21.00 mm, whilst the CFST configuration yields 16.84 mm a reduction of approximately 19.8%. Across all three loading configurations, the CFST system consistently produces lower mid-span deflections than the corresponding CHS models.

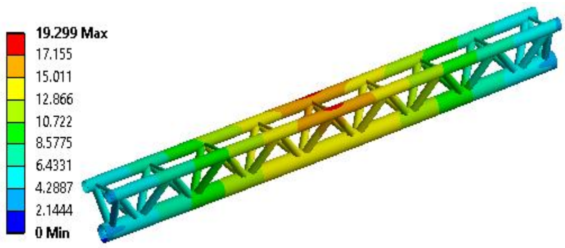

(a) CHS Warren Truss-M11 under mid-point load

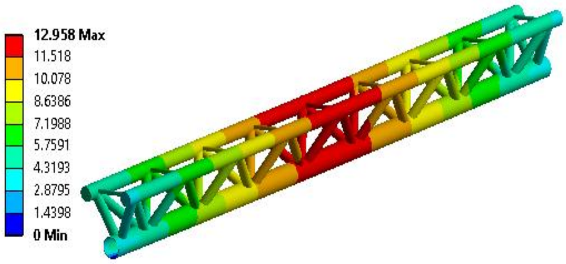

(b) CFST Warren Truss-M11 under mid-point load

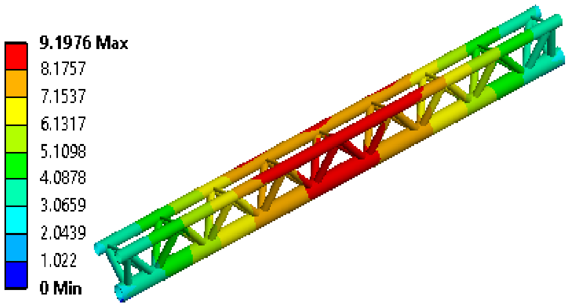

(c) CHS Warren Truss-M11 under two-point load

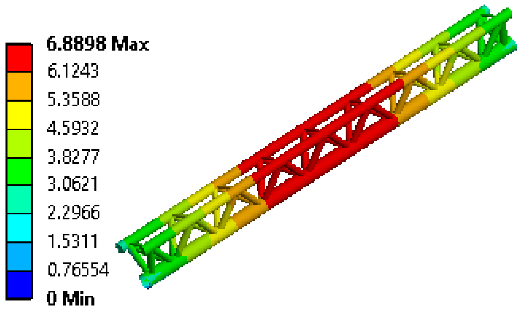

(d) CFST Warren Truss-M12 under two-point load

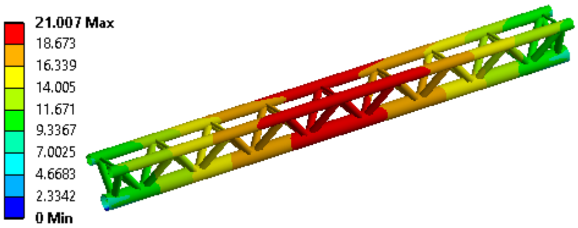

(e) CHS Warren Truss-M13 under UDL

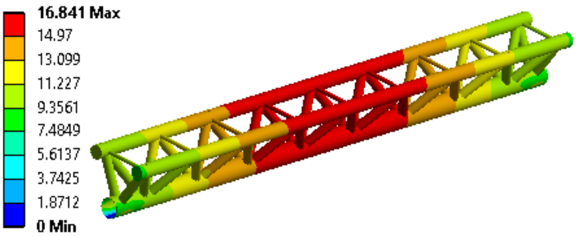

(f) CFST Warren Truss-M13 under UDL

Figure 9. Mid-span deflection of CHS and CFST sections

It is evident from both the theoretical and FEA results that the deviations of 7.5–16.4% between the two approaches are primarily attributable to the idealized pin-jointed and full-bond assumptions of the analytical model, which neglect semi-rigid joint behaviour, partial interface slips at the steel concrete boundary and localized deformation effects at the load application points, as demonstrated by Han et al. (2014). Incorporating a partial interaction factor as per Eurocode 4 (2004), a joint rigidity correction and Timoshenko beam theory in place of the Euler–Bernoulli assumption, as established by Timoshenko and Gere (2012), would be expected to reduce these deviations to within 8–10%.

6.2 Effect of Von Mises Stress in CHS and CFST Sections

Figure 10 shows that peak Von Mises stress locations vary between CHS and CFST configurations depending on the loading condition, reflecting their distinct load transfer mechanisms.

Under mid-point loading, peak stress in the CHS configuration (Figure 10 a) localizes at mid-span chord and diagonal members due to combined bending moment and shear; in the CFST configuration (Figure 10 b), the increased flexural rigidity of concrete-filled chords redistributes stress away from mid-span towards the support connections at the bottom chord. Under two-point loading and UDL, peak stress in the CHS configuration concentrates at the bottom chord between load points (Figure 10 c) and at both mid-span and support connections (Figure 10 e), respectively, reflecting maximum bending and combined bending-shear demands; in both cases, the CFST configuration shifts peak stress towards the support connections and chord ends (Figures 10 d and 10 f), confirming consistent stress redistribution regardless of loading arrangement. Under UDL, the stress concentration zone is broader, engaging more chord and diagonal members due to the distributed bending demand across the full span. Across all loading configurations, the CFST system consistently shifts peak stress from mid-span members towards support connections and chord ends.

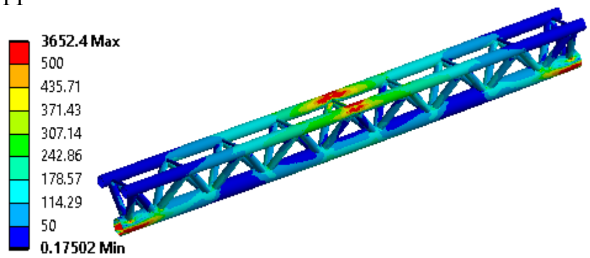

(a) CHS Warren Truss-M11 under mid-point load

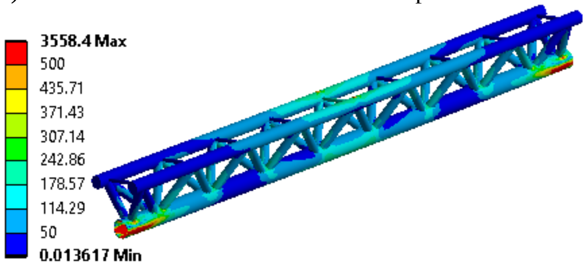

(b) CFST Warren Truss-M11 under mid-point load

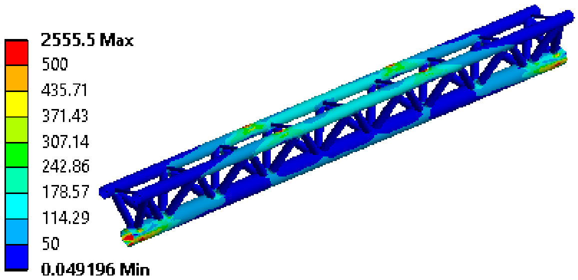

(c) CHS Warren Truss-M12 under two-point load

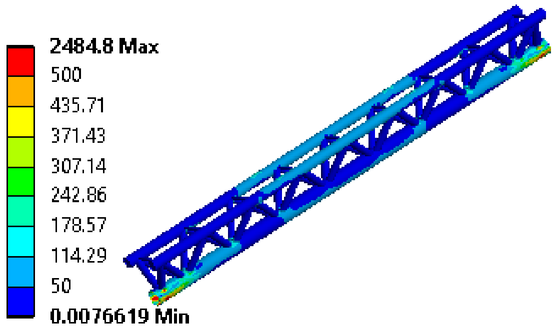

(d) CFST Warren Truss-M12 under two-point load

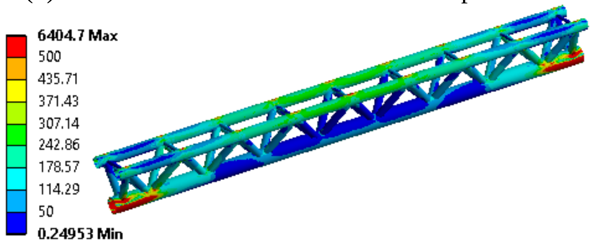

(e) CHS Warren Truss-M13 under UDL

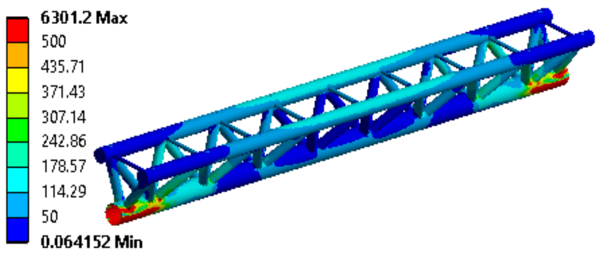

(f) CFST Warren Truss-M13 under UDL

Figure 10. Von Mises Stress contours for CHS and CFST Sections

The von Mises stress contours extracted from the ANSYS Workbench post-processor for the CHS and CFST configurations under different loading conditions indicated that the highest stress concentrations occurred at the nodal joint regions, particularly at the intersection of the diagonal braces with the bottom chord. This is consistent with prior studies on CHS welded truss joints, which have identified the chord crown and the brace-to-chord weld toe as critical stress concentration regions susceptible to fatigue and fracture initiation. Notably, as observed from Figures 10, the average Von Mises stress across all configurations are ranging between 242.86 - 307.14 MPa which remains below the yield strength of steel at 310 MPa, confirming that the truss system operates within the elastic range under the applied loading conditions. Furthermore, the von Mises contours in the CFST models demonstrated a more uniform stress distribution across the chord member length, with reduced stress gradients at the nodal joints compared to the CHS models. This improvement is attributable to the increased local stiffness provided by the concrete-filled chord members at joint locations, which effectively suppresses stress localization and promotes a more favorable load distribution throughout the truss system.

It is noticed from the Figure 10 that the peak von Mises stress varies between 2484 to 6404 MPa are reported at load point and supports and are attributed to stress singularities and not an indicative of material failure. These localized values are excluded from structural performance assessment, which is based on stress results extracted from regions demonstrating mesh independent convergence, consistent with established FEA practice (Cook et al., 2007)

6.3 Nonlinear Analysis of CFST Sections to Estimate Load carrying Capacity

The nonlinear FEA of the CFST sections were conducted using ANSYS Workbench to determine the load capacities, wherein the steel was modelled using a Bilinear Isotropic Hardening plasticity model with an elastic modulus of 210 GPa and a yield strength of 310 MPa, while the concrete infill was represented through the Drucker-Prager plasticity model with a compressive strength of 30 MPa. Bonded contact was established at the steel-concrete interface to enforce full composite action and the boundary conditions from the preceding linear analysis were retained. The deflections of 19.48 mm, 9.48 mm and 21.29 mm obtained from the linear analyses under mid-point, two-point and UDL loading, respectively, were imposed as prescribed displacement boundary conditions, enabling the nonlinear solver to trace the full load-displacement response up to and beyond the elastic limit. The resulting load-displacement curves exhibited a characteristic bilinear behaviour, beginning with a linear-elastic phase in which the steel tube and concrete core act compositely, followed by a gradual stiffness reduction as the concrete core approaches its compressive capacity through microcracking and softening, while the steel tube transitions into the elastic-plastic regime.

Figure 11 presents a nonlinear finite element analyses of the CFST Warren truss under mid-point, two-point and UDL loading produced maximum mid-span deflections of 19.48 mm, 9.48 mm and 21.29 mm, respectively, consistent with the prescribed displacement boundary conditions imposed from the preceding linear analyses.

The von Mises stress contours revealed peak stresses of 5,304.4 MPa, 3,420.7 MPa and 7,966.9 MPa for M11, M12 and M13, respectively, localized at the support bearing regions in all three cases. These values substantially exceed the defined material yield strength of 310 MPa however, this is attributable to classical stress singularities inherent to point-supported FEA models, wherein reaction forces concentrated over a single node produce theoretically unbounded stress values consistent with Saint-Venant's Principle, whereby the stress field recovers to physically realistic values away from the singularity. The chord and diagonal web members across the span remained within expected elastic plastic stress ranges, confirming that the elevated support stresses represent a localized numerical artefact rather than global material failure.

The load carrying capacities of the CHS and CFST sections under different loading conditions were determined from the peak reaction obtained via force reaction probes scoped to the prescribed displacement boundary conditions in ANSYS Workbench and are summarized in Figure 12 and Table 4. Under mid-point loading (M11), the CHS and CFST configurations attained ultimate loads of 238.25 kN and 355 kN respectively, representing a strength improvement of 49.0%, primarily attributed to the concrete infill suppressing local inward buckling of the compressed chord and the confinement induced enhancement of the concrete core compressive strength. Under two-point loading (M12), ultimate loads of 177.97 kN and 245 kN were recorded for the CHS and CFST configurations respectively, yielding a strength enhancement of 37.7%, where the concrete infill provided sufficient internal restraint across the constant bending moment zone to suppress the coupled bending-buckling failure mode governing the bare CHS response. Under UDL (M13), ultimate loads of 474.55 kN and 600 kN were recorded for the CHS and CFST configurations, respectively, representing a yield strength enhancement of 26.4% for the CFST configuration over its CHS counterpart.

Table 4. Comparison of ultimate load-carrying capacity of CHS and CFST Warren truss configurations

Model	Mid Span Deflection (mm)		Load Carrying Capacity, kN		Strength Improvement (%)
	CHS	CFST	CHS	CFST	
M11	19.29	19.48	238.25	355	49.0
M12	9.19	9.48	177.97	245	37.7
M13	21.00	21.29	474.55	600	26.4

The finite element results obtained in this study demonstrate close agreement with the analytical solutions, with deviations maintained within 7.5–16.4% across all Warren truss configurations and loading conditions, confirming the reliability and predictive accuracy of the adopted numerical modelling framework. While experimental investigation remains the most direct means of capturing true structural behaviour, it is associated with several inherent limitations that render finite element analysis the preferred methodology for the systematic parametric study conducted in this work. Adopting the same modelling methodology, material definitions, boundary conditions and loading configurations established and validated for the M1 group, similar analyses were subsequently conducted for the M2, M3 and M4 Warren truss configurations

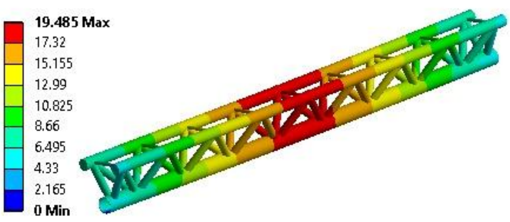

(a) Mid-span deflection for M11

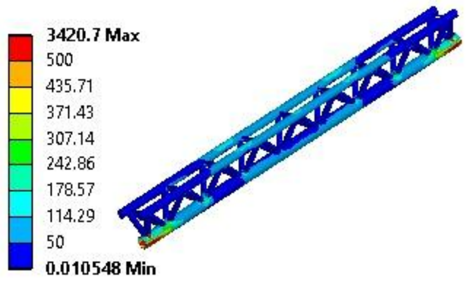

(d) Von Mises Stress Contour for M12

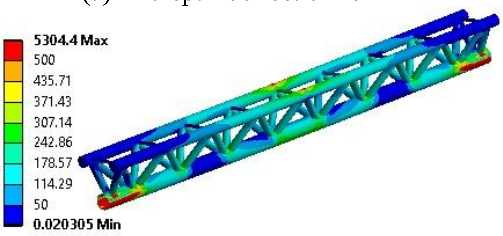

(b) Von Mises Stress contour for M11

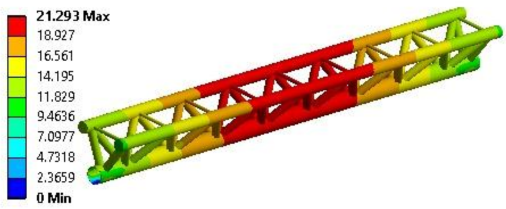

(e) Mid-span deflection for M13

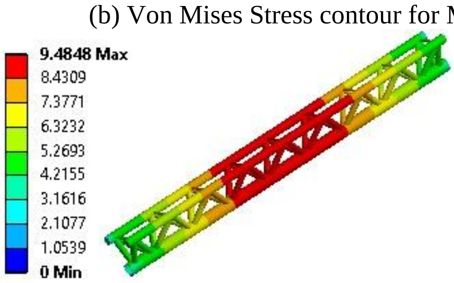

(c) Mid-span deflection for M12

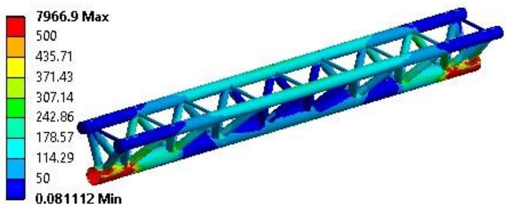

(f) Von Mises Stress Contour for M13

Figure 11. Mid span deflection and Von Mises Stress in CFST Sections

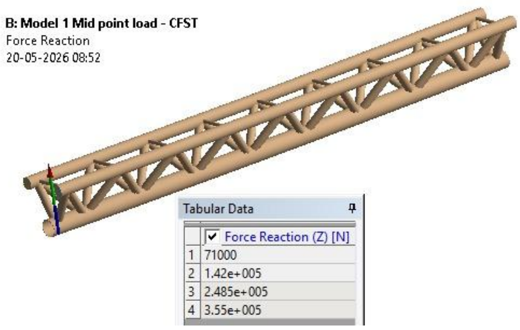

(a) Load carrying for M11

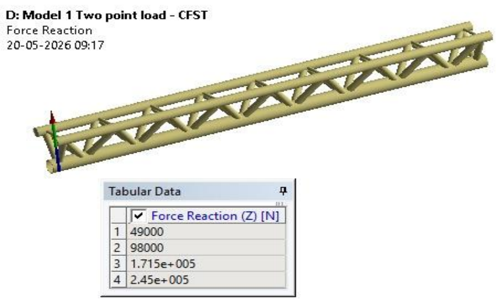

(b) Load carrying for M12

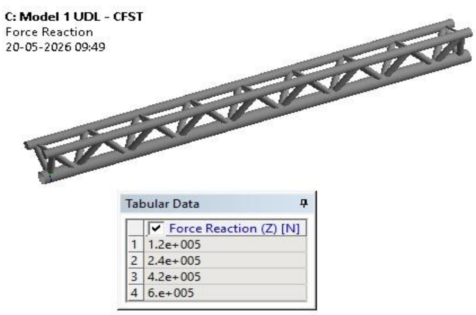

(c) Load carrying for M13

Figure 12. Load carrying capacity of CFST sections

Table 5. Comparison of ultimate load-carrying capacity of CHS and CFST Warren truss configurations

Model	Mid Span Deflection (mm)		Load Carrying Capacity, kN		Strength Improvement (%)
	CHS	CFST	CHS	CFST	
M21	26.23	24.51	269.53	285	5.73
M22	15.10	14.44	202.15	210	3.88
M23	32.65	31.93	539.05	555	2.95
M31	15.64	15.19	171.70	175	1.92
M32	6.46	6.41	128.78	130	0.9
M33	15.2	15.05	343.4	350	1.92
M41	26.5	25.2	352.30	375	6.44
M42	17.45	15.85	262.90	275	4.96
M43	39.82	39.26	701.03	730	4.13

It is evident from Table 5 that CFST configurations exhibited consistently higher load-carrying capacity and lower mid-span deflections than their CHS counterparts across all models. The maximum strength improvement of 6.44% was recorded in Model M41, while the minimum improvement of 0.90% was observed in Model M32, with their respective load-carrying capacities.

In terms of deflection performance, the maximum reduction of 9.17% was recorded in Model M42, while the minimum reduction of 0.77% was observed in Model M32.

The M4-series demonstrated enhanced load-carrying capacity and overall deflection reduction, attributable to its geometric configuration wherein the increased top and bottom chord diameters reduce the effective brace height, thereby producing a stiffer composite section with a greater concrete infill volume; the M2-series, by contrast, exhibited the highest individual strength improvement, reflecting the significant influence of cross-sectional geometry on the degree of composite behaviour.

The M3-series consistently recorded the lowest improvements across both performance indicators, a behaviour directly attributed to its compact cross-sectional geometry, which restricts the effective confinement zone and limits the volume of concrete available for composite load sharing.

The concrete infill volume is one of the primary factors governing the degree of composite action and structural enhancement in CFST members, and the results collectively validate the structural superiority of CFST members over their hollow CHS counterparts.

7. CONCLUSION

This study presents a finite element investigation comparing von Mises stress, deflection, and load-carrying capacity of CHS and CFST Warren truss configurations under different load scenarios across twelve parametric models grouped by sectional area ratio ($2A_1/A_2$) and depth-to-thickness ratio (h/t), conforming to Tata Structura specifications (IS 4923).

Theoretical mid-span deflections ranged from 7.96–18.95 mm for CHS and 5.92–14.97 mm for CFST configurations, reflecting stiffness improvements of 21–37.6%. FEA deflections ranged from 6.46–39.82 mm (CHS) and 6.41–39.26 mm (CFST), with theoretical-to-FEA deviations of 7.5–16.4%, attributable to idealized pin-jointed and full-bond assumptions that neglect semi-rigid joint behaviour and partial interface slip.

Average von Mises stresses across all configurations ranged between 242.86 MPa and 307.14 MPa, remaining below the yield strength of 310 MPa, confirming elastic-range structural safety. CFST models exhibited more uniform stress distributions with reduced stress gradients at nodal joints relative to CHS sections.

Nonlinear analysis yielded load-carrying capacities of 355 kN, 245 kN, and 600 kN under different loading for the M1 group, representing strength improvements of 49.0%, 37.7%, and 26.4% over the equivalent CHS system. The load carrying capacity improvements across all the models ranging from 0.90% (Model M32) to 6.44% (Model M41) and mid span deflection reductions ranging from 0.77% (Model M32) to 9.17% (Model M42), governed primarily by concrete infill volume and cross-sectional geometry, which collectively dictate the degree of composite action and confinement efficiency across all truss series.

Nomenclature

ω_1	:	Unit weight of steel
ω_2	:	Unit weight of concrete
A_1	:	Area of each top chord
A_2	:	Area of bottom chord
b	:	Width between of top chords
C1, C2… C6	:	Total compression
CFST	:	Concrete Filled Steel Tube
CHS	:	Circular Hallow Steel
CIDECT	:	Committee for International Development and Education on Construction of Tubular Structures
d	:	Depth of truss
D_b	:	Diameter of bottom chord
D_{HB}	:	Diameter of horizontal braces
D_{IB}	:	Diameter of inclined braces
D_t	:	Diameter of top chord
E		Youngs Modulus
EAA	:	Equal area Axis
FEA		Finite Element Analysis
h	:	Vertical distance from the centre of the circle to the extreme fibre (used in defining geometric conditions like h < t or h > t).
L		Span
L_i & L_h	:	Length of inclined and horizontal braces
L_t & L_b	:	Length of top and bottom chord
M		Moment of Inertia
M_R	:	Moment of resistance
t	:	Thickness of chord
T, T1 … T3	:	Total Tension
W_{DL}	:	Dead Load
W_{LL}	:	Live Load
$y_1, y_2 … y_{12}$	:	Distances from centroid to EAA
δ	:	Deflection

References:

Abdelaal, A. H., Radwan, T. H., & Shaat, A. A. (2024). Experimental and numerical investigations of double bracket to CHS column joints. *Scientific Reports*, *14*(1), 27115. https://doi.org/10.1038/s41598-024-77646-6

Al Zand, A. W., Badaruzzaman, W. H. W., Ali, M. M., Hasan, Q. A., & Al-Shaikhli, M. S. (2020). Flexural performance of cold-formed square CFST beams strengthened with internal stiffeners. *Steel and Composite Structures*, *34*(1), 123. https://doi.org/10.12989/scs.2020.34.1.123

AlObaidi, S. M., Mousa, M. A., Almusawi, A. M., Shallal, M. A., & Alzabeebee, S. (2024). Flexural Behavior of Concrete-Filled Steel Tube Beams Composite with Concrete Slab Deck. *Infrastructures*, *9*(10), 187. https://doi.org/10.3390/infrastructures9100187

American Institute of Steel Construction [AISC] (2010). *AISC design guide 24: Hollow structural section connections*. Chicago, IL, USA.

American Institute of Steel Construction [AISC] (2016). *ANSI/AISC 360-16: Specification for structural steel buildings*. Chicago, IL, USA.

Beck, A. T., De Oliveira, W. L., De Nardim, S., & ElDebs, A. L. (2009). Reliability-based evaluation of design code provisions for circular concrete-filled steel columns. *Engineering Structures*, *31*(10), 2299–2308. https://doi.org/10.1016/j.engstruct.2009.05.004

Chen, S., Hou, C., Zhang, H., & Han, L. (2019). Structural behaviour and reliability of CFST trusses with random initial imperfections. *Thin-Walled Structures*, *143*, 106192. https://doi.org/10.1016/j.tws.2019.106192

CIDECT. (2008). *Design guide for circular hollow section (CHS) joints under predominantly static loading.* Geneva, Switzerland.

Cook, R. D., Malkus, D. S., Plesha, M. E., & Witt, R. J. (2007). *Concepts and applications of finite element analysis*. John Wiley & Sons.

European Committee for Standardization. (2004). *EN 1994-1-1: Eurocode 4 – Design of composite steel and concrete structures*. Brussels, Belgium.

European Committee for Standardization. (2005a). *EN 1993-1-1: Eurocode 3 – Design of steel structures*. Brussels, Belgium.

European Committee for Standardization. (2005b). *EN 1993-1-8: Eurocode 3 – Design of joints*. Brussels, Belgium.

Han, L., Li, W., & Bjorhovde, R. (2014). Developments and advanced applications of concrete-filled steel tubular (CFST) structures: Members. *Journal of Constructional Steel Research*, *100*, 211–228. https://doi.org/10.1016/j.jcsr.2014.04.016

Han, L., Xu, W., He, S., & Tao, Z. (2015). Flexural behaviour of concrete filled steel tubular (CFST) chord to hollow tubular brace truss: experiments. *Journal of Constructional Steel Research*, *109*, 137–151. https://doi.org/10.1016/j.jcsr.2015.03.002

Hou, C., Han, L., & Zhao, X. (2013). Concrete-filled circular steel tubes subjected to local bearing force: Experiments. *Journal of Constructional Steel Research*, *83*, 90–104. https://doi.org/10.1016/j.jcsr.2013.01.008

Hu, B., Che, R., Wang, J., He, X., Li, L., & Kundu, T. (2023). Analytical investigation into the *flexural behavior of steel tubular truss-and-concrete (STTC) composite beams. Structures, 50, 670–688. https://doi.org/10.1016/j.istruc.2022.11.106*

Huang, W., Lai, Z., Chen, B., & Yao, P. (2017). Experimental behavior and analysis of prestressed concrete-filled steel tube (CFT) truss girders. *Engineering Structures*, *152*, 607–618. https://doi.org/10.1016/j.engstruct.2017.09.035

IS 11384 (1985). *Code of practice for composite construction in structural steel and concrete*. New Delhi, India.

IS 4923 (2017). *Hollow steel sections for structural use Specification (2nd rev.)*. New Delhi, India.

IS 800 (2007). *General construction in steel Code of practice*. New Delhi, India.

Machacek, J., & Cudejko, M. (2011). Composite steel and concrete bridge trusses. *Engineering Structures*, *33*(12), 3136–3142. https://doi.org/10.1016/j.engstruct.2011.08.017

Manikandan, K. B., & Umarani, C. (2021). Understandings on the Performance of Concrete-Filled Steel Tube with Different Kinds of Concrete Infill. *Advances in Civil Engineering*, *2021*(1). https://doi.org/10.1155/2021/6645757

Montuori, R., Nastri, E., Piluso, V., & Todisco, P. (2024). Finite element analysis of concrete filled steel tubes subjected to cyclic bending. *Engineering Structures*, *314*, 118364. https://doi.org/10.1016/j.engstruct.2024.118364

Pi, Y., Liu, C., Bradford, M. A., & Zhang, S. (2012). In-plane strength of concrete-filled steel tubular circular arches. *Journal of Constructional Steel Research*, *69*(1), 77–94. https://doi.org/10.1016/j.jcsr.2011.08.008

Premakumar, S. H., Shivaiah, R., & Mallesh, G. (2026). A nonlinear finite element investigation of contact-induced stress and deformation in tubular warren truss structures. *Proceedings on Engineering Sciences*, *8*(1), 405-416. https://doi.org/10.24874/PES08.01A.013

Rabi, M. (2025). Investigation on the Buckling Behavior of Normal Steel CHS Beam–Columns: A Revised Design Approach with Reliability Analysis. *Buildings*, *15*(10), 1708. https://doi.org/10.3390/buildings15101708

Satria, A., Shalihah, A. R., Nurhadi, F. F., Gurning, R. H., & Purbaning, S. P. (2025). Structure analysis of Warren Truss Bridge using 3D CAD software. *Jurnal Inotera*, *10*(2), 241–250. https://doi.org/10.31572/inotera.vol10.iss2.2025.id486

Singh, H., Tiwary, A. K., Eldin, S. M., & Ilyas, R. (2023). Behavior of stiffened concrete-filled steel tube columns infilled with nanomaterial-based concrete subjected to axial compression. *Journal of Materials Research and Technology*, *24*, 9580–9593. https://doi.org/10.1016/j.jmrt.2023.05.135

Tata Steel – Tubes Strategic Business Unit. (2023). *Tata Structura: Hollow steel sections product catalogue*. Mumbai, India: Tata Steel.

Timoshenko, S. P., & Gere, J. M. (2012). *Theory of elastic stability*. Courier Corporation.

Sharath Hanavadi Premakumar
JSS Science and Technology University, Civil Engineering,
Mysuru, Karnataka, India
sharathp@jssstuniv.in
ORCID 0000-0001-7911-2635

Raviraj Shivaiah
JSS Science and Technology University, Civil Engineering,
Mysuru, Karnataka, India
ravirajs@sjce.ac.in
ORCID 0000-0002-5256-8197

Goud Mallesh
JSS Science and Technology University, Mechanical Engineering,
Mysuru, Karnataka, India
mallesh@sjce.ac.in
ORCID 0000-0002-4113-107X